Sources of Thermally Generated Vacancies in Single-Crystal and Polycrystalline Gold*

D. N. SEIDMAN† AND R. W. BALLUFFI†
Materials Research Laboratory and Department of Mining, Metallurgy and Petroleum Engineering, University of Illinois, Urbana, Illinois

(Received 19 April 1963)

The rate at which the equilibrium concentration of vacancies is generated during pulsing to elevated temperatures was studied in gold. Thin single-crystal slabs were gas-pulsed ($\sim$1250°C sec^{-1}) into the range 875–920°C, held for short periods of time, and then down-quenched in order to trap the generated vacancies. The vacancies were detected by precipitating them as observable vacancy tetrahedra. Also, polycrystalline foils (grain radius $\sim$150–175 μ) were electrically pulsed ($\sim 18\times10^3$ °C sec^{-1}) to 653 and 878°C. In this case the generated vacancies were detected by their resistance at 4.2°K. The densities of all possible vacancy sources (specimen surfaces, grain boundaries, subgrain walls, and free dislocations in the usual 3-dimensional network) were measured in the pulsed specimens. Knowing the shape of the thermal pulse, the diffusion problem of the maximum possible inward flux of vacancies from the various sources was solved and compared with experiment. A temperature-dependent monovacancy diffusion coefficient and time-dependent equilibrium boundary conditions at the sources were assumed. The results indicated that (1) free dislocations were the predominant sources; (2) the average free dislocation operated as an efficient source. In fact, the specimen filled up at a rate which was as large as 0.1 to 0.2 of the rate calculated on the assumption that vacancy equilibrium was maintained at all times along all free dislocation cores.

I. INTRODUCTION

POSSIBLE vacancy sources in metal specimens include free surfaces, grain boundaries, subgrain walls (dense planar arrays of dislocations), and free dislocations (in the usual 3-dimensional network). At present, little reliable information is available regarding the relative effectiveness of these possible sources.

The electrical pulsing work of Jackson[1,2] and Koehler[2] and Lund[3,4a] and Koehler[4a] pioneered the study of vacancy generation at high temperatures in the situation where the specimen is rapidly heated to an elevated temperature, held there for a short time, and then rapidly down-quenched. In this case the lattice is subjected to a large vacancy subsaturation as a result of the rapid heating, and a large driving force for the generation of vacancies exists. These experiments indicated that vacancies were probably generated at free dislocations, but the work was hampered by a poor knowledge of the specimen structure (i.e., grain size, subgrain size, and free dislocation density). Thus, any conclusions regarding the dominant vacancy sources were uncertain. Sizmann and Wenzl[4b] have also electrically pulsed platinum wires in similarly inconclusive experiments.

As an example of other quite different work, Barnes[5a] showed that the free surfaces and grain boundaries in copper containing helium atoms were sources of thermally generated vacancies. However, he found no definitive evidence for free-dislocation-source action. In other experiments, elastic after-effect measurements in silver-zinc alloys have been used by Cost[5b] and Berry[5c] to indicate that dislocations are sources of vacancies. However, their work was also hampered by a lack of knowledge of the specimen structure.

In view of this situation we have studied the rate of generation of vacancies in pulsed gold specimens possessing a known source structure. A technique was developed for thermally gas-pulsing single crystals and clearly distinguishing internally produced vacancies from vacancies generated at the free surfaces. In addition, the Lund-Koehler[3,4a] electrical-pulsing technique was used and extended to study generation kinetics in polycrystalline specimens whose free dislocation density, subgrain size and grain size were measured. Knowing the various source densities the maximum possible generation rates at the possible sources were calculated and then compared with experiment.

Gold was a logical choice for the present study since (1) the high-temperature monovacancy diffusion coefficient and equilibrium vacancy concentration are known (Simmons and Balluffi[6]); (2) vacancy precipitation is readily observable by transmission-electron microscopy; (3) specimens are not significantly contaminated[7,8] by heating and cooling in air.

II. EXPERIMENTAL PROCEDURE

2.1. Specimen Preparation

The single-crystal specimens used in the gas-pulsing experiments were initially grown in the form of 1.27-cm

* Work supported by the U. S. Atomic Energy Commission.
† Now at Department of Materials Science and Engineering, Cornell University, Ithaca, New York.
[1] J. J. Jackson, Ph.D. thesis, University of Illinois, 1960 (unpublished).
[2] J. J. Jackson and J. S. Koehler, Bull. Am. Phys. Soc. **5**, 154 (1960).
[3] C. A. Lund, Ph.D. thesis, University of Illinois, 1964 (unpublished).
[4a] J. S. Koehler and C. A. Lund, in *Proceedings of the International Conference on Lattice Defects in Quenched Metals* (Academic Press, Inc., New York, 1965), p. 1. [b] R. Sizmann and H. Wenzl, Z. Naturforsch. **18a**, 673 (1963).
[5a] R. S. Barnes, Phil. Mag. **5**, 635 (1960). [b] J. R. Cost, Acta Met. **11**, 1313 (1963). [c] B. S. Berry (to be published).
[6] R. O. Simmons and R. W. Balluffi, Phys. Rev. **125**, 862 (1962).
[7] J. A. Ytterhus, Ph.D. thesis, University of Illinois, 1964 (unpublished).
[8] J. A. Ytterhus and R. W. Balluffi, Phil. Mag. **11**, 707 (1965).

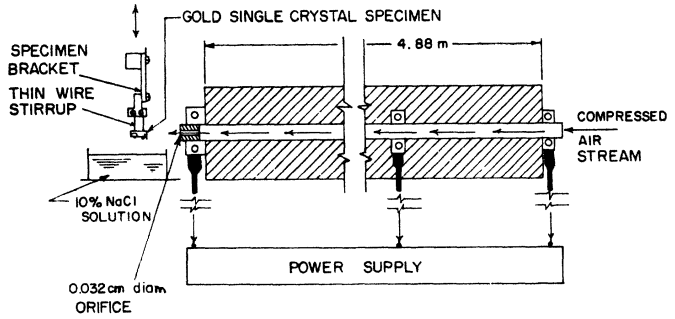

FIG. 1. Schematic diagram of apparatus used to gas-pulse gold single crystals.

cubes using a modified Bridgman technique. The starting material was American Smelting and Refining Company 99.999 weight percent pure gold with a resistance ratio $\mathfrak{R}=R_{25°C}/R_{4.2°K}$ of about 1200. Slabs were then cut out of these crystals with a spark cutter and slowly chemically polished down to dimensions of 0.26 cm×0.051 cm×1.1 cm. The single crystal slabs were then finally annealed at 1025°C for three days in a high-purity-nitrogen atmosphere, except for the last hour which was performed in an oxygen atmosphere in order to purify the crystals (Ytterhus,[7] Ytterhus and Balluffi[8]).

The polycrystalline specimens used in the electrical pulsing experiments were prepared from COMINCO Grade 69 gold of nominal purity 99.9999 weight percent gold. Detectable impurities were 0.1 ppm Cu, 0.1 ppm Mg, and 0.1 ppm Ag. The specimens were received in the form of ribbons 0.018 cm thick, 0.089 cm wide and 18 cm long. The thin rectangular cross section permitted the specimens to be readily electro-thinned for examination by transmission electron microscopy after the electrical resistivity measurements were completed.

For the pulsing and resistivity work, the specimens were mounted on copper frames in the manner described by Ytterhus.[7] Each specimen consisted of a straight gauge length section bounded by two looped end sections which allowed free longitudinal expansion and also promoted a uniform temperature distribution along the gauge length. For the resistivity measurements, fine gold potential lead wires (0.0051 cm diam) were attached at each end of the gauge length. Each specimen was then given a high temperature air anneal by resistance heating it for 2 h in the temperature range 900–1000°C. The air anneal served to purify the gold, promote grain growth, reduce the free dislocation density and sinter on the potential leads. Resistance ratios $\mathfrak{R}$ between 4000 and 5500 were consistently obtained by the above procedure. Care was taken to slowly cool from the annealing temperature in order to avoid trapping vacancies (see thesis of Bass[9]). Also, great care was taken to maintain specimen purity at every stage.

[9] J. Bass, Ph.D. thesis, University of Illinois, 1964 (unpublished); C. P. Flynn, J. Bass, and D. Lazarus, Phil. Mag. 11, 521 (1965).

2.2. Pulsing Techniques

The apparatus used to gas-pulse and water-quench the single crystal slabs is shown schematically in Fig. 1. A rapid jet of hot (875–920°C) compressed air was produced by forcing air through a resistance heated inconel tube 4.88 m long. The specimen was lightly held in a thin wire stirrup which could be quickly pivoted into and out of the hot air beam and directly quenched into a cold brine solution. The history of the thermal pulse produced by this technique was measured by using a dummy specimen with a Chromel-Alumel thermocouple embedded in it. An oscillogram of the thermocouple emf for a typical pulse is shown in Fig. 2. (a).

The upquenching portion of the thermal pulse was exponential and is described by the equation

$$T(t)=T_0+\Delta T(1-e^{-\delta t}), \tag{1}$$

where T_0 is room temperature, ΔT is the temperature interval over which the single crystal was pulsed, t the time in sec and δ the rate constant. A typical value of δ for a 0.05-cm-thick crystal was 5.5 sec^{-1}. The downquenching rate was 1.0 to $1.5\text{–}10^4$°K sec^{-1}.

After downquenching, the single crystals were annealed for 24 h at 60°C in order to precipitate any excess vacancies as stacking fault tetrahedra. The specimens were subsequently observed by transmission electron microscopy.

The polycrystalline foils were electrically pulsed from an initial temperature (T_i) to a final temperature (T_f) in 10 to 20 msec and held at T_f for times ranging from 20 msec to 1.5 sec and then downquenched. The circuit used to accomplish the pulsing and quenching was almost identical to the one employed by Lund.[3] The specimen was made one arm of a Wheatstone Bridge, and the bridge balance at T_f was observed on an oscilloscope. The specimen resistances at T_i and T_f were read by the ammeter-voltmeter method using $\frac{1}{4}\%$ accuracy meters. The specimen could be brought to temperature at the rate of $15\text{–}20\times10^3$°K sec^{-1} by placing a copper fuse wire in series with the specimen. The fuse resistance was adjusted so that it burned out when the specimen reached T_f, and this procedure simply served to bring the specimen to temperature. Once the specimen was at temperature, a battery supplied the

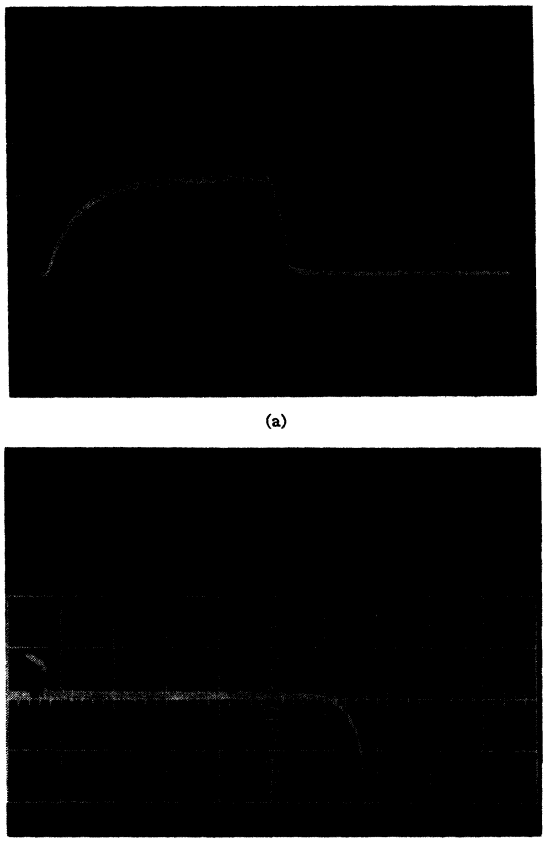

(a)

(b)

FIG. 2. (a). An oscillogram of a gas pulse from room temperature to 875°C. One cm on the horizontal scale corresponds to 0.5 sec. (b). A typical oscillogram of an electrical pulse. One cm on the horizontal scale corresponds to 20 msec, while one cm on the vertical scale is 7.5°C. The portion of the trace to the left of the pip (and including the pip) occurs while the specimen temperature is rising from T_i to T_f, and is an attenuated signal.

necessary heating current. The specimen was automatically released into the quenching bath after any desired time at temperature (T_f) by means of a timed relay. The voltage drop across the Wheatstone Bridge was used to record the specimen temperature-time history. A typical oscillogram is seen in Fig. 2b. The total fractional error ($\Delta R_T/R_{25°C}$) in resistance measurement caused an error of ±3.7°C at 653°C and ±4.5°C at 878°C. The resistance ratio $R_T/R_{25°C}$ was used to convert resistance readings into °C. The temperatures were obtained from the data of Meechan and Eggleston.[10]

After each specimen was downquenched it was cooled by lowering it, within 30 sec, into a vertical test tube almost completely immersed in liquid nitrogen. Any vacancies generated during the pulse were detected by residual resistance measurements at 4.2°K. These measurements were made using the standard potentiometric method with the specimen immersed in liquid helium. The specimen current was obtained by potentiometrically measuring the voltage drop across a standard resistance and the specimen voltage drop was measured potentiometrically across the potential leads. Use of a Rubicon 6-dial potentiometer allowed measurements to $\pm 10^{-12}$ Ω cm. All precision resistance measurements at room temperature were made using the same method, but with the specimen immersed in a constant-temperature water bath.

2.3. Measurement of the Dislocation Density, Subgrain Size, Grain Size

The dislocation density of the polycrystalline foils was measured in electrolytically thinned sections by transmission electron microscopy at a standard magnification of 15,000×. In the present work the dislocation density is taken to be the density of free dislocations and does not include dislocations grouped in well-defined subgrain walls. The density (total line length cm^{-3}) was determined from the relationship, $N_d = 2N_1/A_1$, where N_1 is the number of free dislocations making intersections with both surfaces in an area A_1 (Smith and Guttman,[11] Frank,[12] Ham and Sharpe[13]). All micrographs were taken in relatively thick sections of the specimens, as far from the tapered edge as possible. At least ¾ of each total specimen gauge length was sampled, and several mm of gauge length were electropolished away before each new microscope specimen was cut. In addition, each specimen was tilted in the microscope until the maximum number of dislocations appeared.

The subgrain size was determined by the standard back-reflection Laue x-ray technique and also by the Schulz method. The Schulz patterns were taken of all specimens using white radiation from a fine focus x-ray source (a Hilger microfocus unit with a 40 μ focal spot). In the Laue method the average subgrain area $\bar{A}_2$ is given by A_2/N_2 (Smith and Guttman[11]) where A_2 is the irradiated area and N_2 is the number of subspots within a main Laue spot. It was then assumed that a satisfactory geometrical model for a subgrain is a sphere, and thus, the average radius was given by $(\bar{A}_2/\pi)^{1/2}$. Since a Schulz pattern is merely a magnified Laue spot, the average subgrain cross-sectional area and radius were obtained in this method by the same procedure.

The grain size of the polycrystalline specimens was obtained by standard optical metallographic techniques. In this case the average cross-sectional grain $\bar{A}_3$ is again given by $\bar{A}_3 = A_3/N_3$ where N_3 is the number of grains measured in an area A_3. The grains did not always occupy the full cross section of the foil. Therefore, the grains were represented by cylinders of radius $(\bar{A}_3/\pi)^{1/2}$ and height L'. One flat surface of the cylinder represented the specimen free surface and the other flat surface represented a grain boundary parallel to the

[10] C. J. Meechan and R. R. Eggleston, Acta. Met. 2, 680 (1954).

[11] C. S. Smith and L. Guttman, J. Metals 5, 85 (1953).
[12] F. C. Frank, Proc. Phys. Soc. (London) B70, 1022 (1957).
[13] R. K. Ham and N. G. Sharpe, Phil. Mag. 6, 1193 (1961).

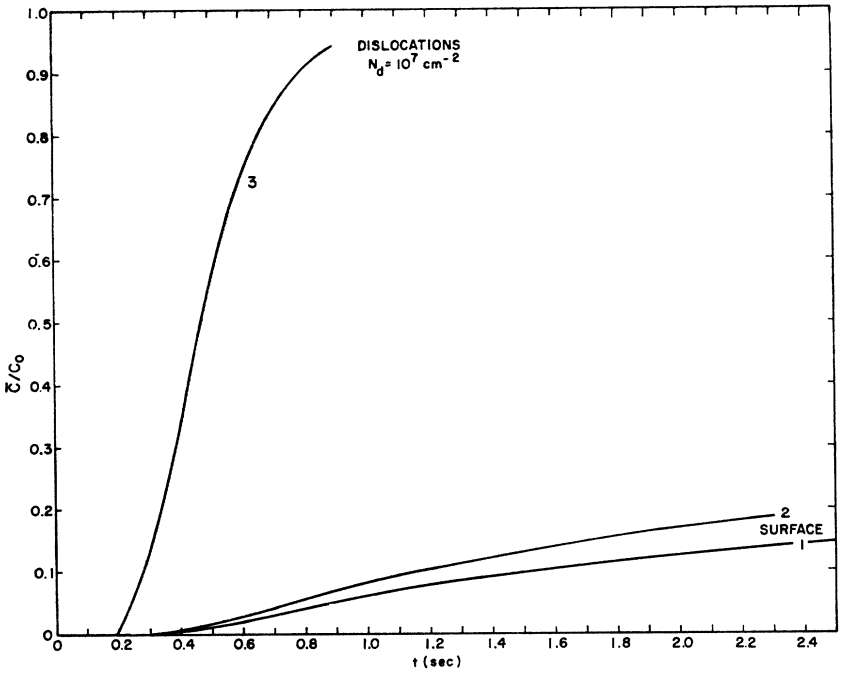

FIG. 3. Calculated mean vacancy concentration $[\bar{C}(t)/C_0]$ versus time for various vacancy sources. Curves 1 and 2 are for 0.5-cm thick slabs at 875 and 900°C, respectively. Curve 3 is for a dislocation density of 10^7 cm^{-2} at 875°C. These curves are based on the calculations discussed in Appendix I.

free surface. The curved surface of the cylinder represented the transverse grain boundaries bounding the grain. The values of the subgrain radii for both twinned and untwinned grains are listed in Table II. An average value for L' of 127 μ was obtained from measurements on transverse cross sections.

III. EXPERIMENTAL RESULTS

3.1. Pulsing of the Single Crystals

The most important initial question regarding vacancy generation is whether the predominant sources are internal or external. This question was answered by the thermal pulsing experiments with the single crystals. After the pulse and annealing treatment each single-crystal specimen was thinned so that the central plane could be examined by electron microscopy. In all of the specimens listed in Table I uniform dense distributions of vacancy tetrahedra were always found in the central plane. In addition, the tetrahedron densities were similar over the range of a factor of 2.5 in the equivalent time at temperature t_{eq} (see Table I for the definition of this parameter). Several control specimens were also equilibrated in this temperature range, downquenched, annealed and examined. The control specimens were similar in all respects to the pulsed specimens and contained approximately the same density of tetrahedra after downquenching and annealing. As a further check, the density and mean edge length of the tetrahedra in specimen 2 listed in Table I were measured. The density was 6.10^{15} cm^{-3}, and the mean edge length was 64 Å. The vacancy concentration was therefore $2.48.10^{-5}$ on the assumption that the observed precipitates were simple stacking fault tetrahedra. This result is in excellent quantitative agreement with the results of Siegel[14] who examined vacancy precipitation in quenched gold which was fully equilibrated at the quench temperature.[15] These results indicate that vacancy generation was rapid enough in these pulsed specimens so

TABLE I. Specimen structure and thermal history of pulsed single crystals.

Spec. No.	T_f (°C)	Δt[a] (sec)	t_{eq}[b] (sec)	$C(x=0)$[c] / C_0	Average subgrain radius from Laue spots (μ)
1	917	4	...	...	...
2	919	1.6	1.4	10^{-4}	...
3	876	2.8	1.7	10^{-4}	245
4	906	1.8	1.5	10^{-4}	245
5	892	2.0	1.8	10^{-4}	301
6	871	1.9	1.0	10^{-4}	212
7	919	2.6	2.5	10^{-4}	212
8	889	2.2	2.0	10^{-4}	173
				Grand average =	228

[a] Δt is the total elapsed time between the beginning of the pulse and the time of the start of the downquench.
[b] The parameter t_{eq} is defined as the isothermal diffusion time at T_f required to produce the same amount of diffusion as actually occurred during the time Δt.
[c] $C(x=0)$ is the vacancy concentration in the central plane of the specimen, $x=0$, calculated using Carslaw and Jaeger's (Ref. 18) tabulations and the values of t_{eq}. The quantity C_0 is the equilibrium vacancy concentration at T_f.

[14] R. W. Siegel, Ph.D. thesis, University of Illinois, 1965 (unpublished).
[15] We note that this concentration is less than would be expected from equilibrium vacancy concentration measurements [Simmons and Balluffi (Ref. 6)]. However, Siegel (Ref. 14) has concluded that the tetrahedral defects in quenched gold are not always simple stacking fault tetrahedra.

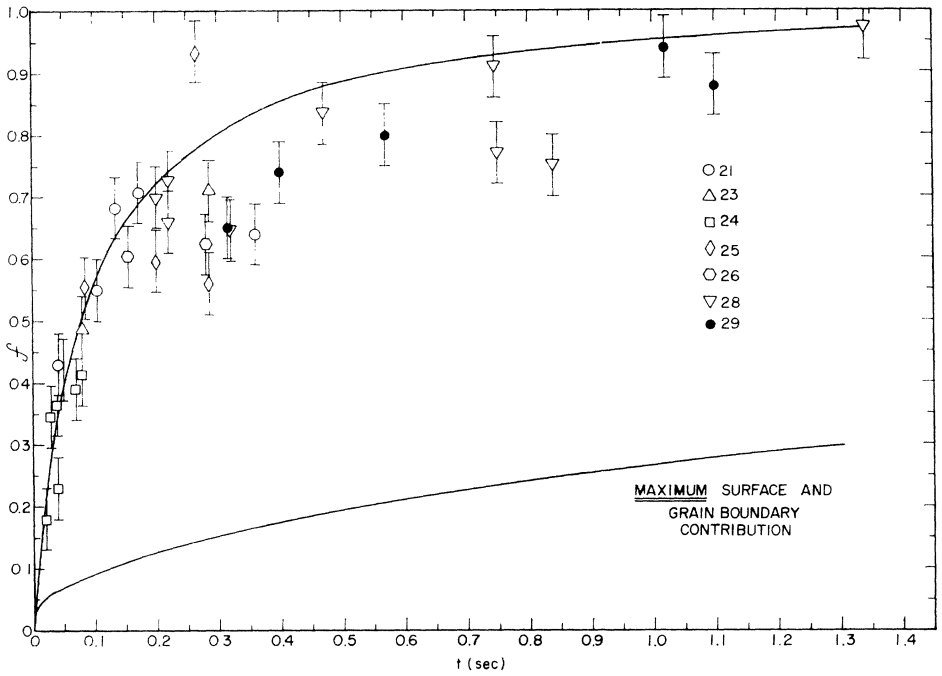

FIG. 4. f versus t for $\bar{T}_f=653$°C and $\bar{T}_i=436$°C. Electrical pulsing technique.

that vacancy equilibrium was attained during the pulsing.

In order to identify the vacancy sources we next solved the diffusion equation for the maximum possible inward flux of vacancies from two possible sources: (1) the exterior surfaces, (2) free dislocations. A temperature-dependent monovacancy diffusion coefficient and time-dependent equilibrium boundary conditions were employed. The calculation for each source was carried out under the assumption that it alone was operating. These assumptions maximized the source effectiveness and therefore yielded an upper limit to the mean vacancy concentration available from a given source. The results[16] for some typical source densities are indicated graphically in Fig. 3. The computed curves for diffusion from the surfaces into the slab were used to determine t_{eq} by comparing these curves with their respective isothermal solutions. For all the equivalent times listed in Table I, the value of $D_{1v}t_{eq}/l^2$ is less than 0.03, where D_{1v} is the monovacancy diffusion coefficient and l the half thickness of the slab. For $D_{1v}t_{eq}/l^2$ equal to 0.03 the vacancy concentration profile is such that $C(x)$[17] is less than $10^{-3}C_0$ for x/l between zero and 0.3 (Carslaw and Jaeger[18]). This result indicates that the observed vacancy concentration in the central plane of the crystal could not have been the result of diffusion in from the free surface. We therefore conclude that the generation must have occurred at either the subgrains or the free dislocations. The results in Fig. 3 show that the free dislocations could easily have maintained the observed generation rates.

3.2. Pulsing of Polycrystalline Specimens

The data in Figs. 4 and 5 represent the vacancy generation kinetics at $\bar{T}_f=653$°C (with $\bar{T}_i=436$°C) and $\bar{T}_f=878$°C (with $\bar{T}_i=653$°C), respectively. The mean fractional vacancy fillup in the lattice at T_f is denoted by

$$f(t)=(\bar{C}(t)-C_i)/(C_0-C_i), \tag{2}$$

where C_i is the initial concentration at $t=0$, C_0 is the equilibrium concentration at T_f, and $\bar{C}(t)$ is the concentration after time t at T_f. Experimentally, the vacancy concentrations were replaced by the quantities $\Delta R/R_{25°C}$ so that Eq. (2) became

$$f(t)=\frac{\Delta R(t)/R_{25°C}-\Delta R_i/R_{25°C}}{\Delta R_0/R_{25°C}-\Delta R_i/R_{25°C}}. \tag{3}$$

The values of $\Delta R_0/R_{25°C}$ and $\Delta R_i/R_{25°C}$ were taken from the recent precise determinations of Bass.[9] The quantity $\Delta R(t)$ was measured at 4.2°K, and the time was read off the oscillogram. The error bar associated with each point reflects the uncertainty in vacancy concentration due to the uncertainty in the temperature T_f.

It is seen that the generation of vacancies occurred without any initial delay period. In addition, the generation occurred very rapidly, but at a rate which

[16] The details of these calculations are given in Appendix I. A further description of the dislocation model employed is given in the Discussion (Sec. IV).

[17] $C(x)$ is the vacancy concentration as a function of position in the single crystal, where $x=0$ is the central plane and $x=l$ is the plane of the outside surface.

[18] H. S. Carslaw and J. C. Jaeger, *Conduction of Heat in Solids* (Oxford University Press, London, 1959), p. 101.

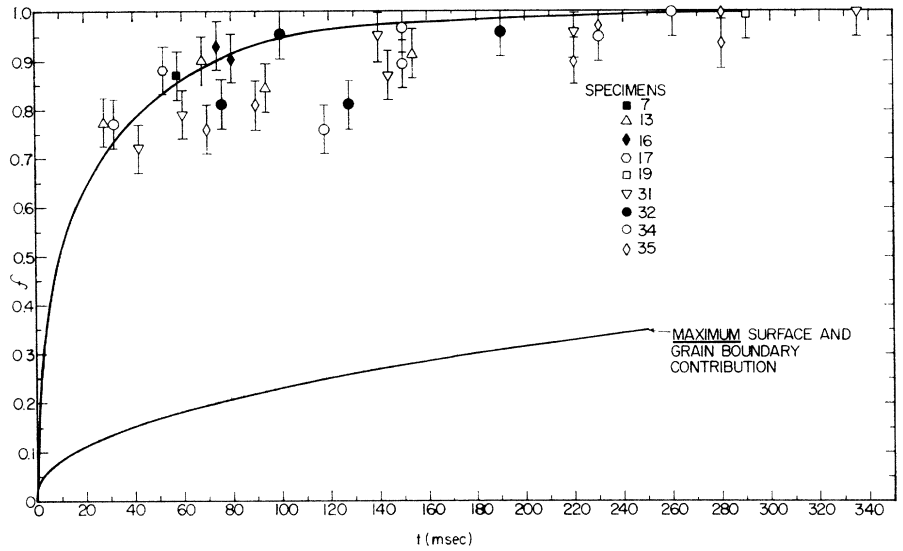

FIG. 5. f versus t for $\bar{T}_f = 878°C$ and $\bar{T}_i = 631°C$. Electrical pulsing technique.

decreased with increasing time. The half-times ($f=0.5$) for vacancy generation were 80 msec and ~9.5 msec at 653°C and 878°C, respectively. We note that the present generation rates agree with those of Lund[3] and Koehler and Lund[4a] to within a factor of about two.

We again calculated the maximum possible inward flux of vacancies from different possible sources using the data for the source densities listed in Table II. The maximum contributions from the surfaces and grain boundaries are shown in Figs. 4 and 5. These curves were computed under the assumption that only these two types of sources could produce vacancies and that they were capable of maintaining local equilibrium at all times. The diffusion equation was solved [19] for the

TABLE II. Structure of electrically pulsed polycrystalline specimens.

Specimen[a] number	N_d (10^7 cm×cm^{-3})	Average subgrain radius from Schulz Patterns (μ)	Average grain radius (μ) (untwinned)[b]	Average grain radius (μ) (twinned)[c]
21	7.9±6.1	111	138	130
24	8.0±4.9	84	170	141
25	6.9±3.8	55	170	153
28	5.2±3.2	62	145	119
29	4.4±2.4	49	210	169
Grand average	6.5±3.2	72	167	142
31	5.5±3.7	52	151	139
32	4.7±3.3	54	195	151
34	4.5±3.0	59	176	152
35	4.5±3.0	60	168	156
Grand average	4.8±3.2	57	173	150

[a] Specimens 21–29 were pulsed to 653°C, and specimens 31–35 were pulsed to 878°C. Each of these specimens had been pulsed and quenched approximately 4 times prior to these measurements.

[b] The untwinned grain radius was determined from the relation $(\bar{A}_3/\pi)^{1/2}$ neglecting the presence of annealing twins. This radius was used in all diffusion calculations.

[c] The twinned grain radius was determined by counting each twinned grain as 2 grains. It is noted that the average grain radius was not radically affected by the presence of the annealing twins.

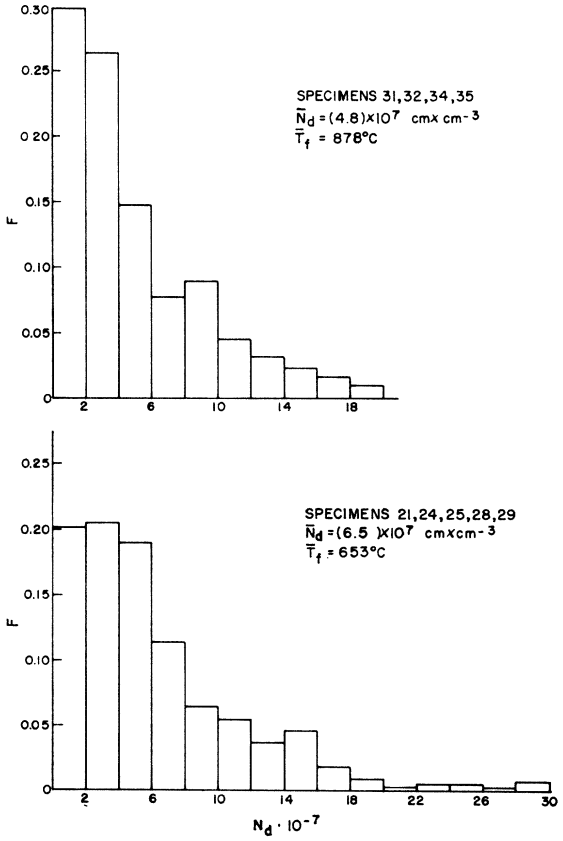

FIG. 6. Histograms of dislocation densities for specimens pulsed to 878 and 653°C. The ordinate F is the fraction of the total photographic plates with a dislocation density N_d.

[19] See Appendix III for the details of the solution.

case of combined radial and axial flow using the radii for untwinned grains listed in Table II and an effective cylinder length (L') of 127 μ. This solution represents an upper limit to the source contribution, since the other internal sources were neglected. At 653 and 878°C the maximum contribution at the half-times was only about $f=0.08$ at both temperatures.

We next considered the possibility that the subgrain walls contributed a significant fraction of vacancies to the observed generation curves. We assumed that only the subgrains were capable of producing vacancies and evaluated $D_{1v}t/a_2^2$ (where a_2 is the subgrain radius) at the observed half-times ($f=0.5$) at both temperatures employing the average values of the measured subgrain radii listed in Table II. This leads to values of 1.3×10^{-3} and 1.5×10^{-3} at 653°C and 878°C, respectively, which makes the maximum possible subgrain contribution about $f=0.12$ at the experimental half-times.

We therefore conclude that the observed generation rate was much too rapid to be explained on the basis of free surface, grain boundary or subgrain sources. The vacancy generation must therefore have been due almost entirely to free dislocations,[20] and this mechanism is therefore discussed in detail below. Before discussing vacancy generation at dislocations however, it is of importance to discuss the following problems which arose in the measurement of the dislocation densities.

3.3. Behavior of Control Specimens

There was some concern that: (1) the free dislocation structures of the specimens could have been altered by the various handling operations before observation in the microscope, and (2) significant free dislocation densities may have been introduced as a result of deformation during certain stages of the pulsing cycle. This would, of course, invalidate any concept of a constant average dislocation source structure in the pulsed specimens. In order to investigate these possibilities, a number of specimens were subjected to various treatments, and their dislocation densities were measured. These data are reported in the form of histograms in Fig. 7(a)–(d).

Before proceeding to the discussion of the control specimens, it is of interest to note that in all the pulsed specimens examined no free dislocations were ever found which had climbed into helical or Bardeen-Herring source configurations.

Specimens 18 and 20 [Fig. 7(a)] were well annealed and slowly cooled to produce $\mathfrak{R}$ values 4295 and 3884, respectively. The mean dislocation density was $(6.3\pm4.1)\times10^7$ cm$\times$cm^{-3}, and the distributions were highly skewed towards the lower densities. This density is seen to be similar to that of the pulsed- and water-quenched specimens, indicating that large dislocation densities were not introduced during the present water quenches. We note that if one attempts to fit the data to a Poisson distribution with the measured variance (mean number of dislocations per fixed area of view), the data do not fit the distribution. The measured distribution contains a larger fraction of low free dislocation density areas than the calculated Poisson distribution. Therefore, we conclude that the free dislocations were nonrandomly distributed in the polycrystalline foils.[21]

To test for the effects of "rough" handling on the measured dislocation densities a specimen was lightly pulled in tension, by hand, at room temperature and its free-dislocation density measured. As Fig. 7(b) indicates, the density was $(1.7\pm0.8)\times10^8$ cm$\times$cm^{-3}, which was the highest of any of the measured densities. There was also considerably more spread in the distribution, and the histogram was no longer skewed towards low densities. This result is consistent with the larger value of the variance in this case. This experiment shows that considerable care must be taken in handling specimens in order to obtain meaningful free-dislocation densities.

As a control on the handling and thinning procedure, two well annealed foils were neutron irradiated with 10^{17} fast neutrons cm^{-2}. A special jig obviated any need to touch the specimens until the electrothinning procedure started. The purpose of the irradiation was: (1) to pin the existing dislocations and hence make their escape from the thinned foil difficult; (2) to raise the yield stress of the specimens, thus making any deformation due to handling more difficult. The results are shown in Fig. 7(c). The dislocation density was $(3.2\pm2.4)\times10^7$ cm$\times$cm^{-3}. This was the lowest measured density, but the mean is still well within the average deviation of the densities measured for the

[20] By sources we mean the *ultimate sources*, i.e., the places where vacancies are generated. In Appendix II it is definitely shown that the dislocations are not merely acting as vacancy pipes with the specimen surface serving as the ultimate source. Therefore, we re-emphasize that the term *source* and *place of generation* are synonymous.

In addition to the above mentioned sources there also exists the possibility of spontaneous homogeneous vacancy generation within the lattice. Koehler and Lund (Ref. 4a) have proposed a *possible* spontaneous vacancy generation model to account for the generation kinetics under the assumption that all the sources which we have considered above are inoperative. They *assert* that thermal fluctuations within the lattice will generate dislocation dipole loops. The geometry consists of a hexagonal interstitial loop containing seven atoms which is separated by one atom layer from a similar hexagonal vacancy loop (see Fig. 3 of Ref. 4a). Vacancies are then generated by lattice atoms jumping into the vacancy loops and shrinking them and also by atoms attaching themselves to the edges of the interstitial loops. The lattice will thus reach the equilibrium vacancy concentration essentially by the growth of the interstitial loops. This implies that the loop radius is essentially zero at $t=0$, and is an increasing function of time during the generation process. This mechanism requires that the vacancy generation curves have the sigmoidal shape of a typical nucleation and growth process. In all the data collected to date (see Figs. 4 and 5 of this paper and Figs. 1 and 2 of Ref. 4a) there is *no evidence* for a sigmoidal shaped generation curve with an inflection point. We must therefore conclude that the self-generation model proposed by Koehler and Lund is incapable of explaining the observed generation kinetics.

[21] This point is discussed more fully in Appendix V.

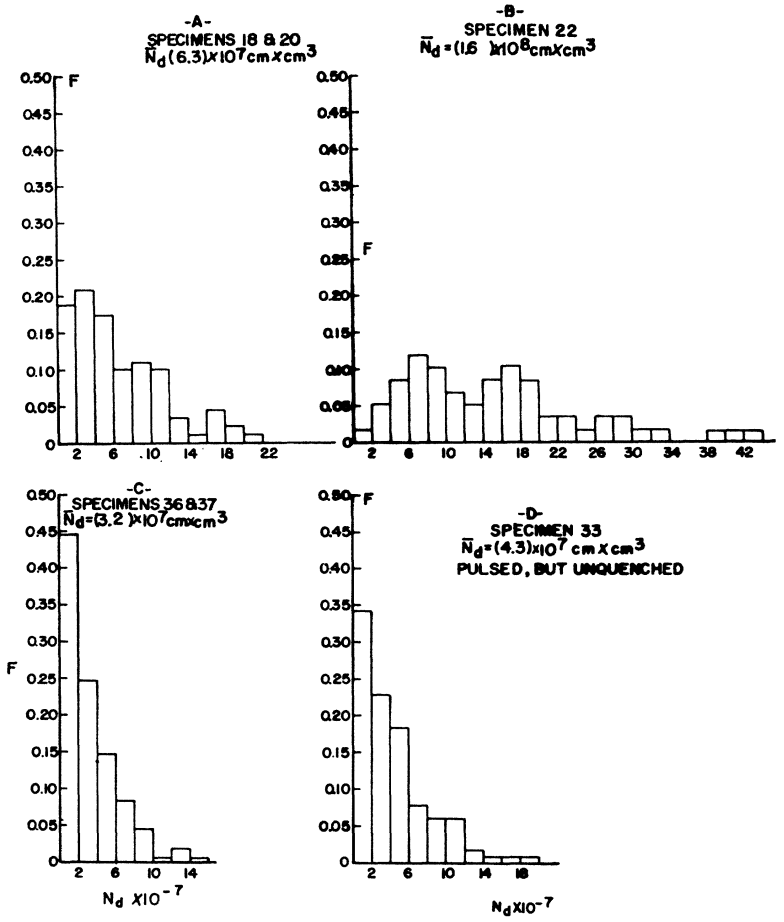

FIG. 7. Histograms of dislocation densities for various control specimens. Graph (a) is for two well annealed gold specimens. Graph (b) is for a specimen deformed lightly in tension. Graph (c) is for two specimens irradiated to 10^{17} *nvt* (fast neutrons). Graph (d) is for spec. 33 which was pulsed but not quenched.

specimens used in the pulsing experiments (see Fig. 6). The histogram is also skewed towards low dislocation densities and does not fit a Poisson distribution with the measured variance of 4.3. This result indicates that densities measured by electron microscopy are probably satisfactory if one observes the precautions described previously.

The final histogram [7(d)] is for specimen 33 which was subjected to a large number of electrical pulses between $T_i \simeq 430°C$ and $T_f \simeq 650°C$. The specimen was first pulsed between these two temperatures several times and then slowly air cooled from 430°C to room temperature. Its resistivity at 4.2°K was then measured. This cycle of multiple pulsing and measuring was then repeated 25 times in all. The resistivity was found to increase continuously by about $\Delta\rho = 2.87 \times 10^{-12}$ Ω cm per cycle. After the 25 cycles the free-dislocation density was measured by microscopy. A value of $(4.3 \pm 3.0) \cdot 10^7$ cm cm^{-3} was found which is within the range of values found previously. If the resistivity increase is attributed to dislocations put in by the pulsing, and if the value of $\Delta\rho$ is converted to dislocation density from the relation $\Delta\rho/N_d = 2.6.10^{-19}$ Ω cm^3 (Basinski, Dugdale, and Howie[22]), then $\sim 3 \times 10^6$ cm×cm^{-3} of dislocations was introduced per pulse. According to this, we might then expect a value of about 3×10^8 cm×cm^{-3} for the free-dislocation density. That this high value was not observed is not surprising as the specimen was annealed during every pulse at the initial temperature (T_i) and also the final temperature (T_f) during the bridge balancing operations. Apparently, the additional dislocations were able to anneal to the subgrain walls. In the walls they contributed to the total resistivity, but not to the measured free-dislocation density.

The above data indicate that some deformation occurred during each pulse, and that a generous upper limit for the number of dislocations introduced per pulse was $\sim 3 \times 10^6$ cm×cm^{-3}. The deformation may be explained on the basis of the well-known Pinch Effect (Northrup[23]), caused by the high current employed during the initial temperature rise. If we take the critical shear stress to cause slip as 2.7×10^6 dynes cm^{-2},

[22] Z. S. Basinski, J. S. Dugdale, and A. Howie, Phil. Mag. 8, 1992 (1963).
[23] E. F. Northrup, Phys. Rev. 20, 474 (1907).

then the minimum current[24] to reach this stress is about 470 A, for the foil geometry employed in the present experiment. Currents of this size were possible in the early portion of the pulses.

There are several important questions that the deformation raises. For example:

(1) How would extra free dislocations introduced during the pulse affect the generation kinetics? Is it possible that a burst of dislocations was injected during the pulse which contributed to the generation rate but annealed out rapidly enough during the pulse to escape final detection?

(2) How many dislocation jogs were created as a result of plastic deformation, and was this jog concentration an appreciable fraction of the thermal equilibrium jog density?

(3) What was the atomic fraction of point defects created by the deformation?

For the low level of deformation involved in this experiment (2) and (3) should have been quite small. But (1) could have been a significant effect, since the generation half-time is expected to be inversely proportional to the free-dislocation density. The possibility that large numbers of dislocations were generated during the pulse and then annealed out during the latter portions of pulse was tested by measuring the free-dislocation densities for pulsed specimens which were not re-annealed at high temperatures (i.e., T greater than 100°C). These data are presented in Table III, and it is seen that each specimen had a density which was within the mean deviation of the grand average for all eight specimens. Therefore, we conclude that for the pulse times of the specimens listed in Table III no detectable concentration of extra dislocations was present. We also recall that a generous *upper limit* to the number of residual free dislocations produced per pulse was only about 3×10^6 cm$\times$cm^{-3}. The work of Young and Savage [25] (on copper) has shown that if N_d is greater than $\sim10^5$ cm^{-2} extensive polygonization may be expected, and an appreciable fraction of the dislocations will remain trapped in low-energy configurations. It is felt in general, that the measured free dislocation densities (see Fig. 6) represent reasonably good average values for the densities in the specimens during the pulses.

TABLE III. Dislocation density as a function of pulse time.

Specimen number	T_f (°C)	t[a] (msec)	$\bar{N}_d\cdot10^{-7}$ [b] (cm cm^{-3})
24	652	80	(8.0±4.9)
25	654	200	(6.9±3.8)
28	658	680	(5.3±3.2)
29	660	745	(4.4±2.4)
31	879	220	(5.5±3.6)
32	878	100	(4.7±3.3)
34	883	150	(4.5±3.0)
35	879	230	(4.5±3.0)
		Grand average	(5.5±3.4)

[a] t is the time spent by the specimen at T_f.
[b] The values reported are the mean values, and the ± values are the mean deviations.

[24] The derivation of an expression for the critical current to cause slip in a specimen with a rectangular cross section is given in the thesis of Seidman (Ref. 45), University of Illinois, 1965 (unpublished).

V. DISCUSSION

4.1. Vacancy-Diffusion-Limited Dislocation Climb

We begin by attempting to account for the observed vacancy generation rates using the simplest possible model in which the rate-limiting step is the diffusion of vacancies away from the dislocation lines acting as line sources and not the rate of vacancy production at the dislocation cores. We thus assume that the vacancy production rate along the dislocation cores is rapid enough so that the equilibrium vacancy concentration is maintained at a small distance r_0 (taken to be 3 Å) from the core. We also assume monovacancy diffusion and consider all the diffusion to be radial. The assumption of monovacancy diffusion is reasonable (Balluffi, Koehler, and Simmons[26]) since the experiments were conducted at T/T_m (T_m is the melting point) greater than 0.69. We also neglect all vacancy-dislocation interactions (see Appendix IV). The model employs a regular array[27,28] of static dislocations separated by a distance $2R$, where

$$R=1/2(N_d)^{-1/2}. \tag{4}$$

The diffusion equation is then solved for a single dislocation lying along the axis of a cylinder of inner radius r_0 and outer radius R. This cell-type model requires that the normal gradient of the vacancy concentration vanish at $r=R$. The resulting solution (see Appendix IV) is

$$f(t)=1-\exp\,(-\xi\ D_{1v}N_d\,t), \tag{5}$$

where ξ is a geometrical factor. This solution was obtained by assuming that the dislocation lines remained stationary as they emitted vacancies. In reality an actual climb motion occurs, but we have shown elsewhere[29] that this motion can be neglected.

In Figs. 8 and 9, the resulting theoretical curves (II) corresponding to the measured dislocation densities are compared to the best-fit experimental curves (I). It is seen that the calculated generation time required to

[25] F. W. Young and J. R. Savage, J. Appl. Phys. **35**, 1917 (1964).
[26] R. W. Balluffi, J. S. Koehler, and R. O. Simmons, in *Recovery and Recrystallization* (Interscience Publishers, Inc., New York, 1963), p. 1.
[27] A regular array and a random array give similar results within about 10%; see Ham (Ref. 28).
[28] F. S. Ham, J. Appl. Phys. **30**, 915 (1959).
[29] R. W. Balluffi and D. N. Seidman, J. Appl. Phys. (to be published).

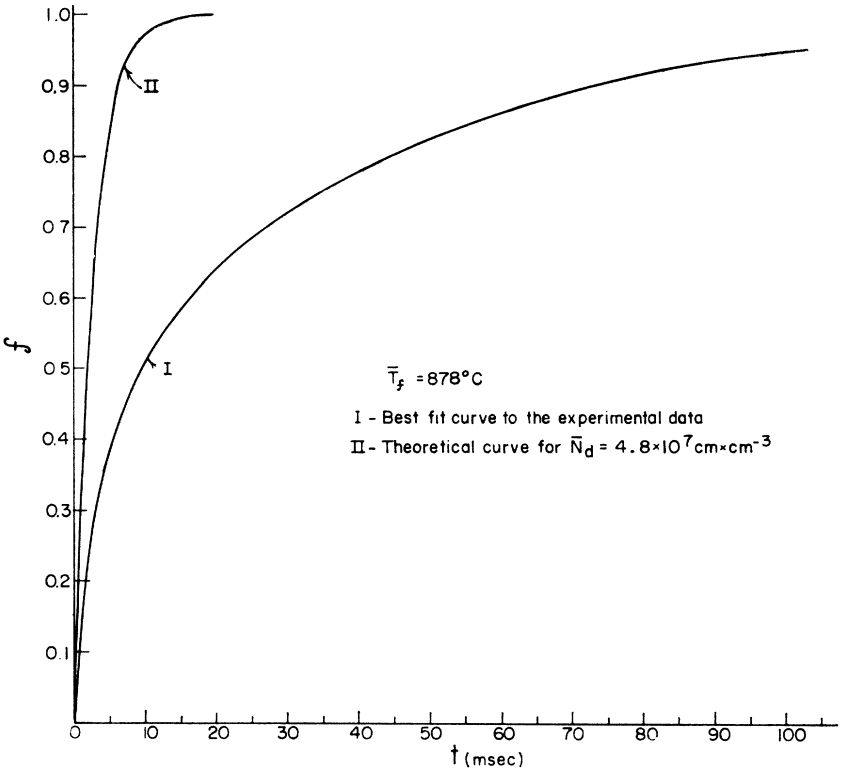

FIG. 8. f versus t (sec) for $\bar{T}_f=653°C$ and $\bar{T}_i=436°C$ (curve I): f versus t for the measured $\bar{N}_d$ using the simple diffusion-limited dislocation climb model (curve II).

reach $f=0.5$ is shorter than the experimental time by a factor of 8, while the time to reach $f=0.9$ is shorter by a factor of 15. At 878°C the corresponding factors are about 5 and 11, respectively. In addition, the observed generation rate decreases more rapidly with increasing time than the calculated exponentially decreasing rate [Eq. (5)]. At least some of this latter difference in behavior is undoubtedly due to the fact that the free dislocations were not randomly distributed throughout the specimens as assumed, but instead were distributed nonrandomly. In a nonrandom distribution appreciable fractions of the volume should have higher and lower dislocation densities than the average density. It is readily shown that this yields a higher initial rate of diffusion-limited generation and a slower rate for the long-time generation than that predicted by the random-distribution model. The histogram data in Figs. 6 and 7 indicate that the free dislocations were actually distributed nonrandomly to at least some extent. In every case the distributions were not Poisson in form and exhibited higher fractions of low-dislocation volumes than a Poisson distribution would predict for the measured variance (see Appendix V). Unfortunately, it was not possible to obtain reliable information regarding the actual dislocation distributions from these measurements. We therefore made no attempt to construct a more realistic diffusion model based upon a nonrandom dislocation array, and we shall be content with Eq. (5) as a first-order solution to the problem. Regardless of the detailed shape of the calculated generation curve, (i.e., the slowdown in the long-time generation rate) we may conclude that the observed rates were considerably slower than the calculated rates.

For purposes of discussion it is convenient to define an average generation efficiency η as

$$\eta=\frac{\text{observed generation rate}}{\text{calculated generation rate for diffusion-limited model}}.$$

The average efficiency, based on the measured free-dislocation densities is as large as 0.1 and 0.2. This result indicates that, while the free dislocations are apparently not perfect line sources, they nevertheless operate as quite efficient sources. It should be emphasized that the above efficiencies are approximate, since the calculated generation rate is based on an obviously approximate model and there is an uncertainly in the total measured dislocation densities (of perhaps a factor of two).

An approximate activation energy (Q) for the fillup of the lattice with vacancies may be determined from

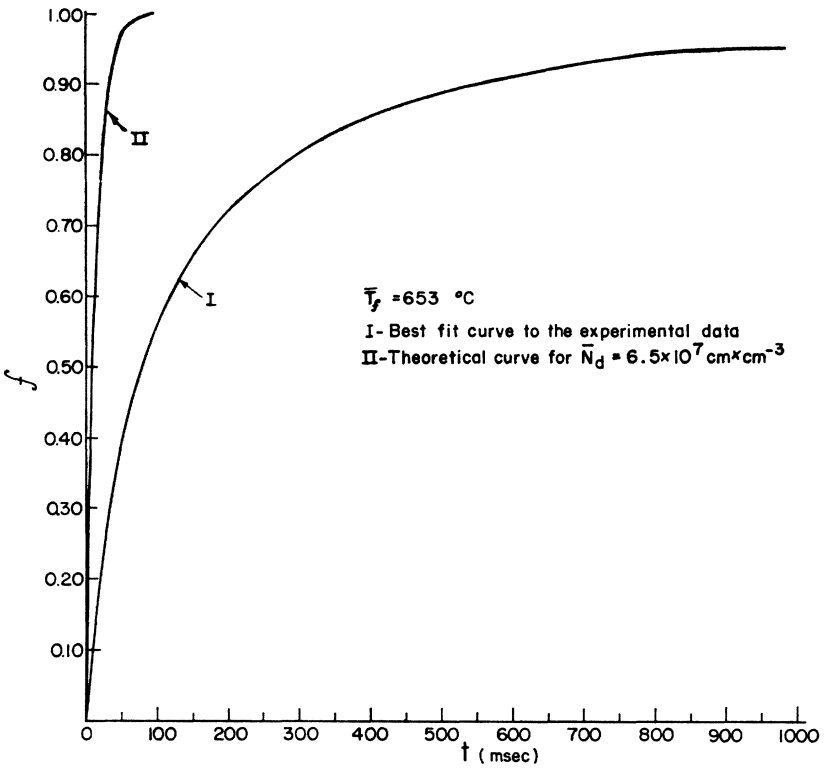

FIG. 9. f versus t (sec) for $\bar{T}_f = 878$°C and $\bar{T}_i = 653$°C (curve I): f versus t for the measured $\bar{N}_d$ using the simple diffusion-limited dislocation climb model (curve II).

the relation

$$\left[\frac{\tau(T_2)}{\tau(T_1)}\right]_f = \exp\left[-\frac{Q}{k}\left(\frac{1}{T_1}-\frac{1}{T_2}\right)\right], \qquad (6)$$

where $T_1 = 653$°C, $T_2 = 878$°C and $\tau(T_2)$ and $\tau(T_1)$ are the corresponding times for the lattice to reach a given value of $f(t)$. This obviously approximate calculation (for ten different values of f) yields activation energies ranging from 1 to 0.8 eV. This result lends support to the idea that we are observing a process which is almost controlled by the rate of diffusion of vacancies from their sources. (The monovacancy migration energy is currently thought to be 0.85 eV.[7–9])

4.2. Vacancy Production Limited Dislocation Climb

The previous results indicate that the vacancy generation rate was limited by the *average* rate of vacancy production along the dislocation cores. The data, of course, describe the generation behavior *averaged over all types of dislocations*. Dislocations with strong edge or strong screw components may climb at quite different rates (Thomson and Balluffi,[30] Escaig[31]). It is, therefore, possible that certain dislocations climbed with almost perfect efficiency. Unfortunately, no detailed information of this type can be gleaned from the present results.

The treatment of vacancy-induced climb is usually couched in terms of jogs, where the vacancies may be easily created or destroyed (e.g., Mott,[32] Weertman[33,34] Lothe,[35] Thomson and Balluffi,[30] Friedel[36]). The continuous production of vacancies causes existing jogs to diffuse along the dislocation cores towards eventual annihilation. In order to maintain a quasisteady state new jobs must be continuously formed and thus the climb rate becomes controlled by the ease of jog formation. Jogs may form either homogeneously or heterogeneously. In the homogeneous case, formation occurs by the nucleation of jog pairs along relatively straight, unperturbed sections of the dislocation lines. In the heterogeneous case the jogs are formed at special sites (i.e., nodes, regions of high curvature, etc.). A basic question is, which of these processes is dominant? Thomson and Balluffi[30] discuss this problem in their treatment of homogeneous climb and conclude that as long as the distance between jogs established by homogeneous processes is small compared to the dimensions of the climbing dislocation line, then homogeneous climb will be dominant. This condition implies a relatively low jog energy, since the jog density tends to increase with decreased jog energy. Thus, an important question to answer is how large may the jog

[30] R. M. Thomson and R. W. Balluffi, J. Appl. Phys. **33**, 803 (1962); J. Appl. Phys. **33**, 817 (1962).
[31] B. Escaig, Acta. Met. **11**, 595 (1963).
[32] N. F. Mott, Proc. Phys. Soc. (London) **B64**, 729 (1951).
[33] J. Weertman, J. Appl. Phys. **26**, 1213 (1955).
[34] J. Weertman, J. Appl. Phys. **28**, 362 (1957).
[35] J. Lothe, J. Appl. Phys. **31**, 1086 (1960).
[36] J. Friedel, *Dislocations* (Pergamon Press, Ltd., London, 1964).

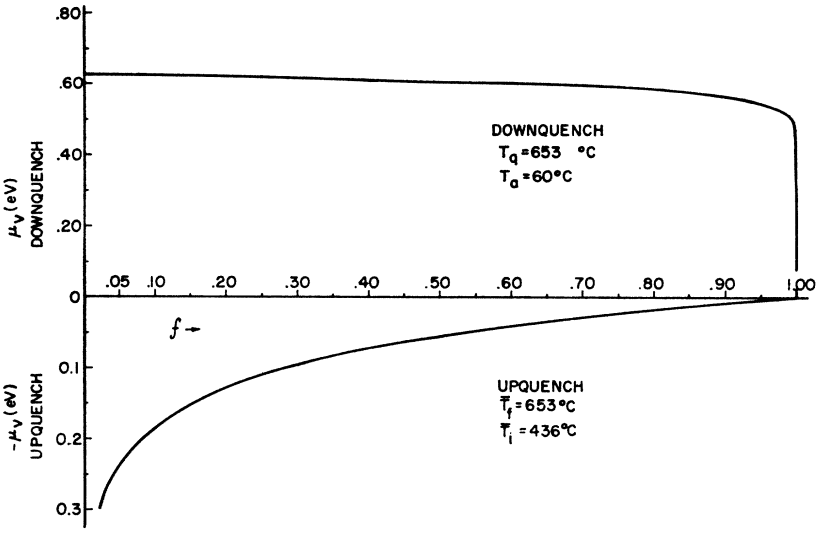

FIG. 10. The vacancy chemical potential μ_v as a function of f for an upquench from 436°C to 653°C and also for a downquench from 653°C to 60°C. For the upquench, f is the fraction of vacancies generated, and for a downquench f is the fraction of vacancies destroyed.

energy become before heterogeneous formation becomes comparable to homogeneous nucleation. Unfortunately, this question cannot be answered since the calculation of the heterogeneous jog formation rate is well beyond our present capabilities. We will therefore give a brief discussion of the homogeneous nucleation case, since we may deal with this problem semiquantitatively.

The problem of homogeneous climb of a straight unconstrained pure edge dislocation has been treated by Thomson and Balluffi.[30] They employ a model in which vacancies are produced at jogs on the dislocation and diffuse rapidly along the line and eventually jump off into the lattice. Detailed expressions are given for the kinetics of this process and also for the rate of formation of jogs on the dislocations. It is shown that the dislocations tend to become more jogged as the subsaturation increases and that the climb rate therefore also tends to increase. In this model, the rate of climb becomes diffusion-limited and the dislocation acts as a perfect line source when the core becomes saturated with vacancies. This situation is aided by a high density of jogs corresponding to a large subsaturation, or alternatively a low jog energy, and a high vacancy diffusivity along the dislocation core. The critical parameters in this model are the degree of subsaturation S, the jog energy E_j, and the distance a vacancy travels along the core before jumping off, α^{-1}. The subsaturation is related to the present parameter f by

$$S=f-1 \tag{7}$$

and is also a measure of the vacancy chemical potential[37] given by

$$\mu_v=kT\ln f=kT\ln(S+1). \tag{8}$$

Physically, μ_v (or S) is a measure of the deviation from equilibrium and measures the driving force for climb. The behavior of this important parameter during the generation process is shown in Fig. 10 for an upquench from $\bar{T}_i=436$°C to $\bar{T}_f=653$°C. For purposes of comparison we have also included a curve for a downquench from $T_q=653$°C (T_q is the quench temperature) to $T_a=60$°C (T_a is the annealing temperature). Of interest is the rapid manner in which μ_v dies off for the upquenched specimen as it equilibrates. On the other hand, μ_v remains essentially constant for the downquenched specimen during the entire annealing process. (We note that the high chemical potential maintained during the entire decay period after downquenching may contribute to the apparent effective dislocation sink action for supersaturated vacancies in quenched gold.[38])

Thomson and Balluffi[30] show that the climb rate is always diffusion limited when

$$\alpha\exp(E_j/kT)<3. \tag{9}$$

Using their expression for α, this relation predicts a jog energy $E_j<0.6$ eV. Since the present data indicate that the climb was production limited, it may be concluded on the basis of this model that $E_j>0.6$ eV. We will not attempt to carry this analysis any further since, as Thomson and Balluffi[30] show, the production limited climb rate is a complex process which depends upon a number of parameters which are presently unknown. For example, the determination of the α parameter depends upon various assumptions regarding the way in which vacancies diffuse along the core. We note that the progressive decrease of the subsaturation seen in Fig. 10 may account for part of the decrease in the observed generation rate which was discussed in (4.1). In this case the decreased subsaturation would decrease the jog density and hence decrease the climb rate.

[37] J. Bardeen and C. Herring, in *Imperfections in Nearly Perfect Crystals* (John Wiley & Sons, Inc., New York, 1952), p. 261.

[38] D. N. Seidman and R. W. Balluffi, Phil. Mag. 10, 1067 (1964).

The present state of knowledge regarding jog energies and defect diffusion along dislocations in face-centered-cubic metals is in a rather poor state. The situation is particularly bad for the low-stacking fault energy metals, like gold, where the equilibrium core and jog configurations are not known.[39,40] For example, Seeger[41] has estimated the jog energy of an edge dislocation in copper to be 4.2 eV. However, Friedel[36] estimated the jog energy to be only $(\frac{1}{10})\mu b^2 d$ (0.92 eV in gold). Here, μ is the shear modulus, b the magnitude of the Burgers vector of the partial dislocations, and d the equilibrium spacing of the partial dislocations. Recently, Escaig[31] has proposed several models for the climb of extended dislocations (also see Thomson and Balluffi[30]) and claims that a dissociated edge dislocation will climb when μ_v is 0.40 eV while partial screw dislocations will climb when μ_v is 0.65 eV. On the experimental side Thornton and Hirsch[42] estimate E_j to be 0.65 ± 0.25 eV from a combination of creep and flow stress data at 300°K. Seeger[41] has estimated from high-temperature creep data that the jog energy is twice Q_l (Q_l is the activation energy for self-diffusion: for gold $2Q_l\sim3.7$ eV). In any case, there is general agreement that the jog energy in a comparatively low-stacking fault metal such as gold should be greater than the jog energy in a high-stacking fault energy metal such as aluminum. It is also possible that defect diffusion along relaxed dissociated dislocations in low-stacking fault energy metals may be slower than along less dissociated dislocations. We therefore predict that the average vacancy generation efficiency of the dislocation network in aluminum, for example, should be at least as high as in gold.

Thus, it is seen that the detailed interpretation of the present observations is quite uncertain because of the great complexity of the dislocation climb process and a lack of information regarding important climb parameters. We may summarize the Discussion with the following:

(1) The free dislocations in the usual 3-dimensional network in gold operated as efficient sources of vacancies under conditions of high vacancy subsaturation during up-pulsing.

(2) The observed rate of generation was as large as 0.1 to 0.2 of the rate calculated on a simple diffusion model where it was assumed that the rate-limiting process was the diffusion of vacancies away from the dislocation cores acting as line sources.

(3) The observed generation rate became particularly slow during the late stages of the generation. This was at least partly due to the fact that the dislocations were nonrandomly distributed and that there were relatively large low-dislocation density volumes present which filled up with vacancies slowly. It is also possible that the progressive decrease in the vacancy chemical potential as the specimen filled up with vacancies contributed to the decrease in the generation rate.

(4) The average vacancy generation rate appeared to be limited by the production rate of vacancies at the climbing dislocation cores rather than by the diffusion rate of vacancies away from them.

(5) Severe problems arose in attempting to describe a realistic detailed model for vacancy production limited dislocation climb. Several aspects of the problems were discussed.

APPENDIX I: SOLUTION OF THE DIFFUSION EQUATION WITH A TEMPERATURE-DEPENDENT DIFFUSION COEFFICIENT AND TIME-DEPENDENT EQUILIBRIUM BOUNDARY CONDITIONS

The general diffusion equation is

$$\partial C/\partial t=\nabla\cdot(D_{1v}\nabla C)\,, \tag{A1}$$

where $D_{1v}=D_{1v}(t)$, so that (A1) becomes

$$\partial C/\partial t=D_{1v}(t)\nabla^2 C\,. \tag{A2}$$

The time-dependent monovacancy diffusion coefficient $D_{1v}(t)$ is given by

$$D_{1v}(t)=D_{01v}\exp[-E_{1v}{}^m/kT(t)] \tag{A3}$$

and $T(t)$ is given by Eq. (1). It is helpful to transform Eq. (A3) according to

$$t'=\int_0^t D_{1v}(t)dt \tag{A4}$$

so that the equation to be solved is

$$\partial C/\partial t'=\nabla^2 C\,. \tag{A5}$$

The solution to Eq. (A5) with time-dependent surface conditions and zero initial concentration within the body is found by applying Duhamel's theorem (Carslaw and Jaeger,[43] Hildebrand[44]). The concentration $[C(x,t')]$ is then given by

$$C(x,t')=\int_0^{t'} F(\tau)\frac{\partial A}{\partial t'}(x,\,t'-\tau)d\tau\,, \tag{A6}$$

where $F(t')$ is the prescribed time-dependent surface concentration, and $A(x,t')$ is the concentration within the body for the condition that $F(t')=1$. The function

[39] In this case the dissociation of the dislocation makes the problem of determining the jog configuration particularly difficult [Hirsch (Ref. 40)].

[40] P. B. Hirsch, Phil. Mag. 7, 67 (1962).

[41] A. Seeger, in *Report of the Conference on Defects in Crystalline Solids* (The Physical Society, London, 1955), p. 30.

[42] P. R. Thornton and P. B. Hirsch, Phil. Mag. 3, 738 (1958).

[43] H. S. Carslaw and J. C. Jaeger, *Conduction of Heat in Solids* (Oxford University Press, London, 1959), p. 30.

[44] F. B. Hildebrand, *Advanced Calculus for Applications* (Prentice-Hall, Inc., Englewood Cliffs, New Jersey, 1964), p. 451.

$A(x,t')$ is obtained from the solution to the diffusion equation with time-independent surface conditions. The function $F(\tau)$ must also be transformed according to Eq. (A4). This is accomplished by finding the inverse $[I^{-1}(t')]$ of Eq. (A4) and using the physical fact that $T(t)=T(\tau)$ so that

$$T(\tau)=T[I^{-1}(t')]. \tag{A7}$$

We are now in a position to find the mean-vacancy concentration $[\bar{C}(t')]$ in the lattice for any possible source. We will only give the solution for the dislocation (using the model described in the text) since the solutions for subgrains and free surfaces are found in an analogous manner and are given in detail by Seidman.[45]

The problem for the dislocation is solved under the boundary conditions:

$$\begin{aligned} C(t)&=\exp(S_{1v}{}^f/k)\exp(-E_{1v}{}^f/kT(t)), \quad t>0, \quad r=r_0,\\ (\partial C/\partial r)&=0, \quad \text{all } t, \quad r=R,\\ C&=0, \quad t=0, \quad r_0<r\leqq R. \end{aligned} \tag{A8}$$

Applying Duhamel's theorem we obtain,

$$C(r,t')=\pi\sum_{n=1}^{\infty}\alpha_n{}^2\int_0^{t'}F(\tau)\exp(\alpha_n{}^2\tau)d\tau\left[\frac{J_1{}^2(R\alpha_n)[J_0(r_0\alpha_n)Y_0(r\alpha_n)-J_0(r\alpha_n)Y_0(r_0\alpha_n)]}{J_0{}^2(r_0\alpha_n)-J_1{}^2(R\alpha_n)}\right]\exp(-t'\alpha_n{}^2) \tag{A9}$$

and then by integration the mean-vacancy concentration is

$$\bar{C}(t')=\frac{2\pi}{R^2-r_0{}^2}\sum_{n=1}^{\infty}\int_0^{t'}F(\tau)\exp(\alpha_n{}^2\tau)d\tau\left[\frac{r_0\alpha_nJ_1{}^2(R\alpha_n)[Y_0(r_0\alpha_n)J_1(r_0\alpha_n)-J_0(r_0\alpha_n)Y_1(r_0\alpha_n)]}{J_0{}^2(r_0\alpha_n)-J_1{}^2(R\alpha_n)}\right]\exp(-t'\alpha_n{}^2), \tag{A10}$$

where the α_n are the roots of

$$Y_0(r_0\alpha_n)J_1(R\alpha_n)-J_0(r_0\alpha_n)Y_1(R\alpha_n)=0. \tag{A11}$$

The $J_n(x)$ and $Y_n(x)$ are Bessel functions of the first and second kind of order n. The eigenvalues α_n are relatively insensitive to the choice of r_0, and a standard value of 3 Å was employed. Equation (A10) was evaluated on an IBM 7094 computer employing the following parameters: $S_{1v}{}^f/k=1.2$ (entropy factor[6]), $E_{1v}{}^f=0.98$ eV (energy of formation of a monovacancy[6,9]), $E_{1v}{}^m=0.85$ eV (energy of migration of a single vacancy[7-9]), $D_{01v}=0.0358$ cm^2 sec^{-1} (pre-exponential factor for monovacancy diffusion coefficient[6,46]) and $\delta=5.5$ sec^{-1}.

APPENDIX II: CALCULATION OF THE DISLOCATION PIPE DIFFUSION COEFFICIENT (D_p) REQUIRED TO MAINTAIN A GIVEN FLUX (ϕ) INTO THE LATTICE

We wish to show that the generated vacancies were not produced at the specimen surfaces and then piped into the specimen via dislocation short circuiting paths. This was accomplished by demonstrating that an impossibly large pipe diffusion coefficient (D_p) was necessary to supply the total *measured* values of the vacancy flux into the specimen.

Consider a pipe of radius r_0 and length Λ to lie along the z axis. The pipe is connected to a source of vacancies at either end ($z=0$ and $z=\Lambda$). The source may be the surface or a grain boundary wall. We then apply the following boundary conditions:

$$C=C_0 \quad \text{at} \quad z=0=\Lambda \tag{B1}$$

$$\partial C/\partial z=0 \quad \text{at} \quad z=\Lambda/2 \tag{B2}$$

$$C=C_0/n \quad \text{at} \quad z=\Lambda/2. \tag{B3}$$

The boundary condition (B3) fixes the deviation from equilibrium where n is any positive number greater than 1. For example, $n=2$ implies that at $z=\Lambda/2$ the vacancy concentration is one-half its equilibrium value C_0.

Consider an element of pipe of length dz and radius r_0. Next we use the equation of continuity to find the steady-state vacancy distribution in the dislocation core along the z axis under the condition that ϕ vacancies cm^{-2} sec^{-1} are leaking out of the element dz of pipe in the r direction. The assumption of a steady-state distribution in the core is reasonable in view of our general requirement that the cores act as essentially constant vacancy sources maintained near the equilibrium concentration and the fact that extremely fast pipe diffusion diffusivities are required. Therefore, the equation of continuity is

$$\frac{\partial C}{\partial t}=D_p\frac{\partial^2 C}{\partial z^2}-\frac{2\phi}{r_0} \tag{B4}$$

which reduces to

$$D_p\frac{\partial^2 C}{\partial z^2}=\frac{2\phi}{r_0} \tag{B5}$$

in the steady state.

Integrating and using boundary conditions (B1) and (B2) yields the steady-state distribution in terms of

[45] D. N. Seidman, Ph.D. thesis, University of Illinois, 1965 (unpublished).

[46] S. M. Makin, A. H. Rowe, and A. D. LeClaire, Proc. Phys. Soc. (London) **B70**, 545 (1957).

D_p, z, and ϕ:

$$C(z)=\frac{\phi z^2}{D_p r_0}-\frac{\phi\Lambda}{D_p r_0}z+C_0. \quad \text{(B6)}$$

Now by applying Eq. (B3), we obtain the pipe diffusion coefficient (D_p) in terms of measurable parameters:

$$D_p=\frac{n\phi\Lambda^2}{4(n-1)C_0 r_0}. \quad \text{(B7)}$$

The vacancy flux ϕ is proportional to the slope of the plot of $f(t)$ versus t (see Figs. 4 and 5), and is given by the expression

$$\phi=\frac{C_0}{2\pi r_0 N_d}\left(\frac{df}{dt}\right). \quad \text{(B8)}$$

The final expression for the required D_p is therefore given by

$$D_p=\frac{n\Lambda^2}{8\pi(n-1)r_0^2 N_d}\left(\frac{df}{dt}\right). \quad \text{(B9)}$$

In Table IV, we present required values of D_p at 653 and 878°C for $n=2$, $r_0=3$ Å and $N_d=3.10^7$ cm cm^{-3} for both the single-crystal and polycrystalline specimens. The measured values of df/dt at $f=0.5$ were used. It is seen that the values of D_p necessary to support the measured values of df/dt are enormous. In the penultimate column we have crudely estimated the required Debye frequency in the pipe for a value of $(E_{1v}{}^m)_p=0.1$ eV[47,48] from the equation

$$D_p=\tfrac{1}{6}d_{112}{}^2 z\nu_p \exp[-(E_{1v}{}^m)_p/kT] \quad \text{(B10)}$$

with $z=10$ and $d_{112}=a_0/\sqrt{6}$ where a_0 is the lattice parameter of gold. Note that the smallest value of ν_p is at least a factor of 10^6 greater than the normal Debye frequency of the lattice. In the last column we have calculated the necessary $(E_{1v}{}^m)_p$ for a more reasonable ν_p of 10^{13} sec^{-1}. The resulting values are seen to be negative. In view of these impossible requirements we conclude that the vacancies are produced internally and are not simply piped into the lattice from the surface via dislocation short circuits. In view of the problem associated with the choice of a model for pipe diffusion we note that the choice of any other reasonable model would lead to essentially the same conclusion.

TABLE IV. Calculated values of the pipe diffusion coefficient (D_p) and other parameters necessary to support the measured vacancy flux (df/dt) in a short-circuiting model.

T_f (°C)	$(df/dt)_{f=1/2}$ (sec^{-1})	Λ (cm)	$D_p\times10^{-8}$ (cm^2 sec^{-1})	$\nu_p\times10^{-19}$ (sec^{-1})	$(E_{1v}{}^m)_p$ (eV)
653	3.3	0.0127	1.5	1.2	−1.0
878	19	0.0127	9	5.5	−1.4
		0.051	145	89	−1.7

APPENDIX III: SOLUTION OF THE DIFFUSION EQUATION FOR COMBINED RADIAL AND AXIAL FLOW FROM THE GRAIN BOUNDARIES AND FREE SURFACE

The general solution for combined radial and axial flow is (Carslaw and Jaeger[49])

$$C(z,r,t)=1-\psi(a,L',t)\zeta(r,a,t). \quad \text{(C1)}$$

$\psi(z,L',t)$ is the function appropriate to the slab $0<z<L'$ with unit initial concentration and with surfaces kept at zero concentration. The function $\zeta(r,a,t)$ is the solution to the diffusion equation for an infinite cylinder with unit initial concentration and zero surface concentration. If Eq. (C1) is integrated over the volume of the cylinder, the mean vacancy concentration as a function of time is

$$f(t)=1-\frac{8}{\pi^2}\sum_{n=1}^{\infty}\frac{[1-(-1)^n]^2}{n^2\beta_n{}^2}\times\exp\left[-D_{1v}t\left(\frac{n^2\pi^2}{L'^2}+\frac{\beta_n{}^2}{a^2}\right)\right], \quad \text{(C2)}$$

where $\beta_n=a\omega_n$ and the β_n are the zeros of the Bessel function $[J_0(\omega_n)]$ of the first kind of order zero.

APPENDIX IV: VACANCY DIFFUSION LIMITED CLIMB

1. Solution of the Diffusion Equation

Under the assumptions given in the discussion we solve the diffusion equation

$$\frac{\partial C}{\partial t}=D_{1v}\frac{1}{r}\frac{\partial}{\partial r}\left(r\frac{\partial C}{\partial r}\right) \quad \text{(D1)}$$

with the following boundary conditions

$$C=C_0, \quad r=r_0, \quad \text{all } t, \quad \text{(D2)}$$

$$C=0, \quad b<r\leqq R, \quad t=0, \quad \text{(D3)}$$

$$\partial C/\partial r=0, \quad r=R, \quad \text{all } t, \quad \text{(D4)}$$

where C_0 is the equilibrium concentration at temperature (T_f). Carslaw and Jaeger[50] have solved the diffusion equation for a hollow cylinder with very general boundary conditions. Restricting their results to our

[47] The value of $(E_{1v}{}^m)_p$ was estimated from the relation $(E_{1v}{}^m)_p=Q_p-(E_{1v}{}^f)_p$, where Q_p is the activation energy for self-diffusion in the pipe and $(E_{1v}{}^f)_p$ is the formation energy of a vacancy in the pipe. The latter quantity is given by $E_{1v}{}^f-E_B$ where E_B is the binding energy of a vacancy to the dislocation core. The value of Q_p was estimated using the relation $Q_p\simeq0.45\,Q_l$ (Ref. 48).

[48] D. Turnbull and R. E. Hoffman, Acta. Met. 2, 419 (1954).

[49] H. S. Carslaw and J. C. Jaeger, *Conduction of Heat in Solids* (Oxford University Press, London, 1959), p. 33.

[50] H. S. Carslaw and J. C. Jaeger, *Conduction of Heat in Solids* (Oxford University Press, London, 1959), p. 332.

boundary conditions yields the solution

$$C(r,t)=1-\pi \times\sum_{n=1}^{\infty}\frac{J_1^2(R\alpha_n)[J_0(r_0\alpha_n)Y_0(r\alpha_n)-J_0(r\alpha_n)Y_0(r_0\alpha_n)]}{[J_0^2(r_0\alpha_n)-J_1^2(R\alpha_n)]} \times\exp(-D_{1v}t\alpha_n^2), \quad \text{(D5)}$$

where the α_n are the roots of the Eq. (A11).

The mean vacancy fraction (f) is found by integrating $C(r,t)$ over the volume of the cylinder, which yields

$$f(t)=1-\frac{4}{R^2-r_0^2}\sum_{n=1}^{\infty}\frac{J_1^2(R\alpha_n)\exp(-D_{1v}t\alpha_n^2)}{\alpha_n^2[J_0^2(r_0\alpha_n)-J_1^2(R\alpha_n)]}. \quad \text{(D6)}$$

The analyses of Ham[28,51] on diffusion limited precipitation make use of the fact that the largest fraction of the concentration decays according to the first term in the eigenfunction expansion. In Eq. (D6) the fraction of the total vacancies contributed by the nth term is given by

$$\frac{4J_1^2(R\alpha_n)}{(R^2-b^2)\alpha_n^2[J_0^2(b\alpha_n)-J_1^2(R\alpha_n)]} \quad \text{(D7)}$$

which yields a value of 0.996 for the lowest order component (α_1) with $N_d=10^7$ cm cm^{-3} and $r_0=3\cdot10^{-8}$ cm. We may therefore safely replace Eq. (D6) by

$$f(t)\simeq 1-\exp(-\alpha_1^2D_{1v}t). \quad \text{(D8)}$$

Next, we define $1/\tau$ by $1/\tau\equiv\alpha_1^2D_{1v}$, which is then written, with the aid of Eq. (5), as

$$1/\tau=4(R\alpha_1)^2N_dD_{1v}=\xi N_dD_{1v}. \quad \text{(D9)}$$

Equation (D9) then takes the form

$$f(t)=1-e^{-t/\tau}=1-\exp(-\xi N_dD_{1v}t). \quad \text{(D10)}$$

2. The Elastic and Electronic Vacancy-Dislocation Interactions

In solving the diffusion problem we have neglected any interaction between the dislocation and the vacancies. Identifiable elastic interactions (e.g., see Cottrell,[52] Bullough and Newman,[53]) have their origins in (1) a size difference between the vacancy and matrix atoms (E_1); (2) an interaction due to the vacancy acting as an inclusion with an elastic modulus different from that of the host crystal (E_2). There is also an electronic interaction (Flynn[54]) which is an oscillatory long-range interaction modified by an $r^{-5/2}$ dependence. It is the aim of this section to show that the present diffusion problem may be treated by neglecting all the interactions and simply using an "effective" dislocation core radius.

First, it is important to determine the magnitude of the interactions. For the elastic interactions E_1 and E_2 the magnitudes are about $-10^{-1}\ \mu V\epsilon$ and $-6.7\times10^{7}\ \mu V$ at a distance of 10 Burgers vectors from an edge dislocation. Here, μ is the shear modulus, V the volume of a vacancy and ϵ, the radial strain due to the relaxation around a vacancy. Using a value of one-half an atomic volume for the volume of a vacancy[6] we find $E_1/E_2=27$, and conclude that the dominant elastic interaction is E_1. The short-range character of the electronic interaction varies as $r^{-5/2}$ while E_1 has an r^{-1} dependence. Therefore, E_1 is again the dominating interaction.

Ham[28] obtained an exact solution for steady-state diffusion to an edge dislocation in the presence of the interaction (E_1). By comparing this solution to the simple solution in the absence of the interaction he was able to define an "effective" capture (emission) radius given by

$$\Phi=\tfrac{1}{4}(Be^{\gamma}/kT), \quad \text{(D11)}$$

where B is a factor made up of elastic constants (Cottrell[52]) and γ is Euler's constant. He justified the use of Φ by solving the time-dependent diffusion equation in the presence of the interaction numerically and comparing it to the analytical solution in the absence of the interaction employing Φ as the radius of the dislocation core. His results indicated that within 10% (at the worst) the solutions were identical. Using measured values of the elastic modulus of gold[55] we find that Φ is about 5 Å at 653°C and 3.4 Å at 878°C. Since the eigenvalue α_1 has a logarithmic dependence[56] on the ratio R/r_0, we conclude that our use of a constant 3 Å core radius was justified.

APPENDIX V: COMMENTS ON THE DISTRIBUTION OF FREE DISLOCATION DENSITIES THROUGHOUT THE SPECIMENS

A short discussion of the statistics involved in the measurement of dislocation densities is presented. The total area that could be sampled in a given polycrystalline specimen was about 0.45 cm^2, while each micrograph sampled only 0.244×10^{-6} cm^2. Therefore, below a dislocation density of about 8×10^6 cm cm^{-3} (i.e., one dislocation per micrograph) the sampling became very difficult. Each distribution was based on 150 to 300 micrographs taken at random in regions away from the thin edges of the foil. Hence, the total fraction of area sampled was 8.2×10^{-5} for each specimen.

The data were plotted in the form of distributions normalized to unity, i.e., in each case the fraction $F(n)$ of the total number of plates with a given number of dislocations (n) was plotted against the number of dislocations. The variance (average number of dislocations

[51] F. S. Ham, J. Phys. Chem. Solids **6**, 335 (1958).
[52] A. H. Cottrell, *Dislocations and Plastic Flow in Crystals* (Oxford University Press, London, 1953), pp. 57, 74.
[53] R. Bullough and R. C. Newman, Phil. Mag. **7**, 529 (1962).
[54] C. P. Flynn, Phys. Rev. **125**, 881 (1962).
[55] W. Köster, Z. Metallkunde **39**, 1 (1948).
[56] The lowest eigenvalue (α_1) is given $\alpha_1^2\simeq(2/R^2)[\ln(R/r_0)-\frac{3}{4}]^{-1}$. See Ham (Ref. 28) for further details.

per micrograph) was determined, and this variance was then used to calculate the expected fraction $f(n)$ on the assumption that the distribution of dislocations obeyed a Poisson distribution. The goodness of fit was then checked using the standard χ^2 test (e.g., Parratt[57]). For example, the distribution for the specimens pulsed to 878°C (see Fig. 6) had a probability of less than 10^{-3} of fitting a Poisson distribution. The main reason for the poorness of the fit is that the measured distribution had a higher fraction of plates with low n values than the calculated Poisson distribution. This result is hardly surprising, since we would expect the dislocations in highly deformed and recrystallized metals to be non-randomly distributed.

[57] L. G. Parratt, *Probability and Experimental Errors in Science* (John Wiley & Sons, Inc., New York, 1961), p. 195.

ACKNOWLEDGMENTS

The authors would like to thank Dr. C. A. Lund and Professor J. S. Koehler for the details of the electrical pulsing circuit, for the loan of equipment, and for helpful advice. Thanks are also due to Dr. Piers B. Bowden for interesting discussions during the course of the investigation. In addition, they would like to thank Cary Conley for assistance with the experimental work and David Hutchinson for programming.

PHYSICAL REVIEW VOLUME 139, NUMBER 6A 13 SEPTEMBER 1965

Electron Emission from Tungsten under Proton Bombardment*

RONALD I. EWING
Sandia Laboratory, Albuquerque, New Mexico
(Received 5 April 1965)

The yield of electrons from clean polycrystalline tungsten under bombardment by protons at normal incidence has been measured as a function of proton energy in the range 50 to 225 keV. The maximum value of the yield is 1.65 ± 0.03 electrons per proton at a proton energy of 125 keV. The tungsten surface was cleaned by flash heating a tungsten ribbon to 2400°K in a vacuum chamber in which the total pressure was about 2×10^{-10} Torr. The yield was measured with the surface at room temperature, about two minutes after the surface was cleaned, while the time for a monolayer of residual gases to form on the surface was greater than two hours.

INTRODUCTION

ELECTRON emission from solids under ion bombardment can supply information about the surface and bulk properties of solids,[1] and is an important phenomenon in gas discharges and in the measurement of ion currents.

The specification of the surface condition of the target during the measurement of γ, the electron yield per incident ion, is of prime importance, since the presence of absorbed gases may strongly influence the observed value.[2] Hagstrum,[3] and Propst and Luscher[4] have demonstrated the effects of monolayer adsorption on electron ejection from tungsten under bombardment by low-energy ions. Large[5] has measured γ for flashed tungsten targets bombarded by protons in the energy range 10 to 140 keV. In his experiments the residual pressure was about 10^{-8} Torr, and the time to obtain a measurement of γ was of the order of the monolayer coverage time.

In the present work γ was measured with an experimental accuracy of 1%. The residual pressure was about 10^{-10} Torr, and measurements were obtained within a time after flash-cleaning that was less than 2% of the observed time for a monolayer of gas to form on the target. At the time of the measurement, the tungsten surface was covered by no more than a few percent of a monolayer of gas. The electron yield γ was observed to depend on surface coverage by adsorbed gas at less than monolayer coverage.

APPARATUS

The essential components of the apparatus are shown in Fig. 1. The energy of the proton beam was determined by measuring the accelerating voltage on the Cockcroft-Walton accelerator to an accuracy of 0.2%. The proton beam entered the measurement chamber through a 0.30-in.-diam canal of length $\frac{3}{8}$ in., which permitted differential pumping between accelerator and chamber. The beam passed through three apertures of diameters $\frac{1}{16}$, $\frac{3}{16}$, and $\frac{1}{8}$ in., respectively, in the plates marked A, B, and C in Fig. 1. Plate A was grounded and restricted the beam size; plate B was biased 600 V negative to repel stray electrons; and plate C was part of the electrode that collected the secondary currents emitted from the target. The targets were

* This work was supported by the U. S. Atomic Energy Commission.
[1] H. D. Hagstrum, Ann. N. Y. Acad. Sci. **101**, 674 (1963).
[2] L. N. Large, Proc. Phys. Soc. (London) **81**, 175 (1963).
[3] H. D. Hagstrum, Phys. Rev. **104**, 1516 (1956).
[4] F. M. Propst and E. Luscher, Phys. Rev. **132**, 1037 (1963).
[5] L. N. Large, Proc. Phys. Soc. (London) **81**, 1101 (1963).

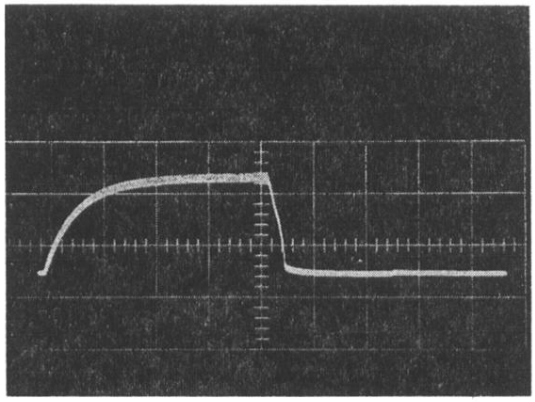

(a)

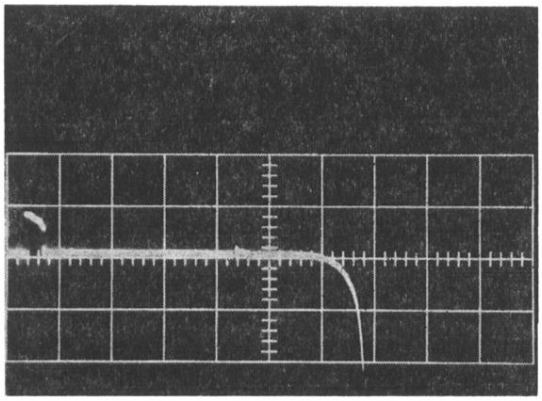

(b)

FIG. 2. (a). An oscillogram of a gas pulse from room temperature to 875°C. One cm on the horizontal scale corresponds to 0.5 sec. (b). A typical oscillogram of an electrical pulse. One cm on the horizontal scale corresponds to 20 msec, while one cm on the vertical scale is 7.5°C. The portion of the trace to the left of the pip (and including the pip) occurs while the specimen temperature is rising from T_i to T_f, and is an attenuated signal.